Microtubule Dynamics Investigated by Microinjection of *Paramecium* Axonemal Tubulin: Lack of Nucleation but Proximal Assembly of Microtubules at the Kinetochore During Prometaphase

G. Geuens,* A. M. Hill,‡ N. Levilliers,‡ A. Adoutte,‡ and M. DeBrabander*

*Department of Cellular Biology and Pathology, Janssen Research Foundation, B-2340 Beerse, Belgium;
‡Laboratoire de Biologie Cellulaire 4, Unité Associé Centre Nacional de la Recherche Scientifique 1134, Université Paris-Sud, 91405 Orsay-Cedex, France

Abstract. Microtubule (MT) dynamics in PtK_2 cells have been investigated using in vivo injection of unmodified *Paramecium* ciliary tubulin and time-lapse fixation. The sites of incorporation of the axonemal tubulin were localized using a specific antibody which does not react with vertebrate cytoplasmic tubulin (Adoutte, A., M. Claisse, R. Maunoury, and J. Beisson. 1985. *J. Mol. Evol.* 22:220–229), followed by immunogold labeling, Nanovid microscopy, and ultrastructural observation of the same cells. We confirm data from microinjection of labeled tubulins in other cell types (Soltys, B. J., and G. G. Borisy. 1985. *J. Cell Biol.* 100:1682–1689; Mitchison, T., L. Evans, E. Schulze, and M. Kirschner. 1986. *Cell.* 45:515–527; Schulze, E., and M. Kirschner. 1986. *J. Cell Biol.* 102:1020–1031). In agreement with the dynamic instability model (Mitchison, T., and M. Kirschner. 1984. *Nature (Lond.).* 312:237–242), during interphase, fast (2.6 μm/min) distal growth of MTs occurs, together with new centrosomal nucleation. Most of the cytoplasmic MT complex is replaced within 15–30 min. During mitosis, astral MTs display the same pattern of renewal, but the turnover of the MT system is much faster (~6 min).

We have concentrated on the construction of the kinetochore fibers during prometaphase and observe that (*a*) incorporation of tubulin in the vicinity of the kinetochores is not seen during prophase and early prometaphase as long as the kinetochores are not yet connected to a pole by MTs; (*b*) proximal time-dependent incorporation occurs only into preexisting kinetochore MTs emanating from centrosomes. Consequently, in undisturbed prometaphase cells, the kinetochores probably do not act as independent nucleation sites. This confirms a model in which, at prometaphase, fast probing centrosomal MTs are grabbed by the kinetochores, where tubulin incorporation then takes place.

A variety of techniques have been applied to the study of the dynamics of microtubule (MT)[1] assembly and disassembly in living cells. The pioneering studies of Inoué and Sato (1967) and others after them, who used polarized light microscopy, have first drawn attention to the remarkable dynamics of MT arrays. Microinjection of labeled tubulin into living cells combined with time-lapse fixation and immunofluorescence or electron microscopy made it possible to locate exactly the sites of incorporation into existing MT complexes and to estimate the time range of MT turnover (Keith et al., 1981; Soltys and Borisy, 1985; Mitchison et al., 1986; Schulze and Kirschner, 1986). Combined with the above techniques, bleaching of specific areas in living cells has been used to gather additional qualitative as well as quantitative information (Salmon et al., 1984; Saxton et al., 1984; Wadsworth and Salmon, 1986; Sammak et al., 1987). Finally, a longstanding dream of many cell biologists has been fulfilled, namely the observation of the growth and shrinkage of single MTs in vitro (Horio and Hotani, 1986) and in living cells, using microinjected rhodamine-labeled tubulin and video-intensified microscopy (Sammak and Borisy, 1988). One of the major conclusions drawn from these studies is that the MT network of several lines of cells in culture exists in a highly dynamic state. The majority of MTs are constantly growing at their tips and new ones are constantly initiated off the centrosomes, implying that an equivalent number of MTs are simultaneously disassembled, in agreement with the "dynamic instability" of MT complexes in vitro (Mitchison and Kirschner, 1984*b*).

We have been attempting to approach the problem of MT dynamics, particularly during mitosis, following the same

1. *Abbreviations used in this paper*: MES, 2-(*N*-morpholino)ethanesulfonic acid; MT, microtubule.

general strategy of *in vivo* injection of a marker tubulin followed by time-lapse fixation. We have used, however, a newly developed tool consisting of unmodified *Paramecium* ciliary tubulin and a polyclonal antibody (Cohen et al., 1982) which reacts strongly with this tubulin but is totally unreactive with vertebrate cytoplasmic or mitotic tubulins (Adoutte et al., 1985). It appeared, therefore, that we might be able to follow specifically the in vivo incorporation of *Paramecium* tubulin into the MTs of a vertebrate cell by using this specific antibody. Such experiments could at least serve the purpose of confirming previous results obtained with chemically modified tubulin.

Furthermore, we aimed at performing these experiments with the best possible method of fixation. Several previous studies have relied on the use of extraction before fixation with the inclusion of so-called MT-stabilizing compounds such as taxol or glycerol (Soltys and Borisy, 1985; Mitchison, 1985). It is not inconceivable that these procedures induce shifts in the equilibrium and thus may lead to erroneous interpretations.

Our major aim was to investigate the origin and construction of the kinetochore fibers. They consist of MTs connecting the chromosomes with the poles (centrosomes), hence the dynamics of kinetochore MTs must play a fundamental role in chromosome movement during mitosis. Detailed ultrastructural analysis had left ambiguity: some MTs go virtually all the way between kinetochores and centrosomes; while others, either connected to the poles or to the kinetochores, seem to terminate somewhere in between (for a review, see Rieder, 1982). If kinetochore MTs are anchored at both ends, they must accommodate length changes as chromosomes move; they have to elongate in the course of prometaphase when chromosomes move away from the poles and congress to the metaphase plate, and they have to shorten during anaphase when chromosomes move back to the poles. The question which is raised is to know where and by which mechanism tubulin subunits are added or lost during these MT length changes. In vitro studies have shown that the kinetochore is able to nucleate MT growth (Mitchison and Kirschner, 1985*a*) and also to cap preformed MTs and allow proximal assembly at the attached end (Mitchison and Kirschner, 1985*b*). Previous microinjection studies have only concentrated on the problem of dynamics at the kinetochore during metaphase and anaphase when the kinetochore fiber is already formed (Mitchison et al., 1986; Gorbsky et al., 1987). They have shown that tubulin can be incorporated into or released from kinetochore MTs at the kinetochore itself. Because of its complexity, the prometaphase situation had not yet been examined. The hypothesis, which we and others have advocated, states that the proven capacity of kinetochores to induce MT assembly (nucleation) in living cells after release from a nocodazole or colcemid block (Witt et al., 1980; De Brabander et al., 1981) is also implicated in the construction of the kinetochore fiber during undisturbed prometaphase (De Brabander, 1982; De Brabander et al., 1986*a*). In other words, we expected that the kinetochore fiber is formed by interdigitating MTs: one set originating at the centrosome and another set originating at the kinetochore. This model predicts that, during prometaphase, exogenous tubulin is incorporated at the kinetochore into newly nucleated MTs that are not yet connected to a centrosome. However, the presently favored hypothesis states that all spindle MTs have originally been nucleated at the centrosomes and that some of them become attached to the kinetochores. In this case, we would expect to see MT assembly at the kinetochore only after the kinetochore has interacted with a centrosomal MT.

In this paper, we show with combined light microscopical and ultrastructural methods (*a*) that *Paramecium* ciliary tubulin is efficiently incorporated into interphase and mitotic MTs; (*b*) that our results are qualitatively and quantitatively similar to those published previously; and (*c*) that tubulin is only incorporated into MTs at a kinetochore when a kinetochore fiber is already connected to it and no assembly or nucleation of MTs is seen before this occurs.

Materials and Methods

Strains and Culture Conditions

Paramecium tetraurelia cells, wild-type stock d4-2 (Sonneborn, 1974) were grown at 27°C in phosphate- and Tris-buffered wheat grass infusion (Pines Distributors International, Lawrence, KS), bacterized with *Aerobacter aerogenes*, and supplemented with 0.4 μg/ml β-sitosterol (Sonneborn, 1970), to yield at least 5,000 cells/ml in stationary phase.

For immunoblotting, rat kangaroo epithelial (PtK_2) cells were cultured in RPMI medium (Flow Laboratories, Puteaux, France) supplemented with 10% FCS (Eurobio, Paris, France). For the microinjection experiments, PtK_2 cells were cultured in MEM supplemented with nonessential amino acids and 10% FCS.

Preparation and Assembly of Paramecium Axonemal Tubulin

Batches of 15-liter cell suspension were concentrated by continuous flow centrifugation in a chemical centrifuge (International Equipment Co., Needham Heights, MA) and harvested by centrifugation at 200 *g* for 1 min in pear-shaped vessels in a centrifuge (Giovanni Giaccordo, Torino, Italy).

Cells were deciliated as described by Cohen et al. (1982). They were briefly washed with 10 mM $MnCl_2$ and resuspended in 20 vol 10 mM $MnCl_2$ supplemented with protease inhibitors (20 μg/ml leupeptin and 1 mM PMSF) for 15 min, a time sufficient to cause immobilization of nearly all cells but not cell lysis. The progress of deciliation was monitored by observation under a phase-contrast microscope. Cilia were then freed from cell bodies by two centrifugation steps at 850 *g* for 1 min and then 4 min. All operations up to this point were carried out at room temperature. Subsequent steps were performed at 0–4°C. Cilia were recovered from the supernatant by centrifugation at 17,000 *g* for 10 min (SS-34 rotor; RC2-B centrifuge; Sorvall Instruments, Newton, CT).

Ciliary membranes were removed by resuspension of ciliary pellets for 15–30 min on ice in demembranation buffer (10 mM Tris-maleate, 3 mM EDTA, pH 7.2, supplied with 1% [vol/vol] Triton X-100, 1 mM DTT, 40 μg/ml leupeptin, and 1 mM PMSF), in a final volume of 2 ml for 6 ml starting packed cells in a typical preparation.

After pelleting at 17,000 *g* for 10 min, axonemes were resuspended, in a volume of 1 ml/ml packed cells, in a low ionic strength buffer (1 mM Tris-HCl, 0.1 mM EDTA, 0.1 mM EGTA, 1 mM DTT, 1 mM NaN_3, pH 7.8), adapted from Linck and Langevin (1981), and supplemented with 40 μg/ml leupeptin and 1 mM PMSF before dialysis for 18 h against the same buffer devoid of protease inhibitors. Doublet MTs were sedimented at 150,000 *g* (60 Ti rotor, L5-65 ultracentrifuge, Beckman Instruments Inc., Palo Alto, CA) and were either further processed or stored at −80°C until further use.

For microinjections, sonication was carried out in injection buffer containing 20 mM Na-glutamate, 1 mM EGTA, 1 mM $MgCl_2$, pH 6.8. Alternatively, for self-assembly studies, MT pellets were suspended in a sonication buffer containing 10 mM 2-(*N*-morpholino)ethanesulfonic acid (MES), 1 mM EGTA, 1 mM $MgCl_2$, 1 mM DTT, 2 mM GTP, pH 6.8, according to Linck and Langevin (1981). MT pellets were taken up in a minimal volume (50 μl/ml packed cells) in order to provide a maximal protein concentration (1–10 mg/ml). They were sonicated in a melting ice-water bath at least by 5 × 1-min sonication bursts at 100 W separated by 1-min intervals, or continuously for 3 min followed by 3 × 1-min pulses, using a Cleanet sonifier (H. Grieshaber AG, Zürich, Switzerland). The progress of sonica-

tion was followed by electron microscopic observation of negatively stained aliquots. The suspension was centrifuged at 350,000 *g* (TLA-100.1 rotor, TL-100 tabletop ultracentrifuge, Beckman Instruments, Inc.) and yielded solubilized tubulin in the supernatant. The latter could be frozen as aliquots in liquid nitrogen and stored until use. After thawing, aliquots were never frozen for a second time.

Reassembly of the axonemal tubulin 350,000 *g* supernatant was carried out by addition of 10-fold-concentrated reassembly buffer, yielding final concentrations of 20 mM MES, 2 mM EGTA, 10 mM $MgCl_2$, 0.15 M KCl, 1 mM DTT, 3 mM GTP at pH 6.4 or 6.8. Polymerization was initiated by warming to 37°C and checked by electron microscopic observation of negatively stained material.

Coassembly experiments were carried out using a procedure adapted from Kristofferson et al. (1986). A mixture of 10 μl of 6 μM *Paramecium* axonemal tubulin in buffer A (50 mM MES, 1 mM EGTA, 6 mM $MgCl_2$, 1 mM GTP, 30% glycerol, pH 6.8) with 2.5 μl of 40 μM phosphocellulose-purified porcine brain tubulin in buffer B (80 mM Pipes, 1 mM EGTA, 1 mM $MgCl_2$, 1 mM GTP, pH 6.8), kindly provided by C. Simon and Dr. D. Pantaloni (Labo D'Enzymology, Centre Nacional de la Recherche Scientifique [CNRS], Gif-Sur-Yvette, France), and 7.5 μl of buffer B was pre-equilibrated for 1 min at 37°C. Assembly was initiated by addition of 1 μl of porcine brain MT seeds (70 μM in buffer B with 30% glycerol and 10 μM taxol, prepared by C. Simon), and stopped by addition of 0.5% glutaraldehyde in buffer A plus buffer B (50:50). After centrifugation onto coverslips, the samples were then processed for double-label immunofluorescence, using the rabbit antiaxonemal tubulin antiserum and a purified sheep polyclonal antibody (10 μg/ml) raised against porcine brain tubulin (Hill et al., 1981).

Purification of Antiaxonemal Tubulin Antibodies

The preparation of the antiserum raised against *Paramecium* ciliary tubulin has been previously described (Cohen et al., 1982; Adoutte et al., 1985). Because of background fluorescence obtained on glutaraldehyde-fixed PtK_2 cells with this antiserum, polyclonal rabbit antibodies were affinity purified according to Füller et al. (1975) on a matrix containing sonication-solubilized *Paramecium* axonemal tubulin, prepared as described above and coupled to CNBr-activated Sepharose 4B (Pharmacia Fine Chemicals, Lesulis, France) (1.7 mg tubulin/0.3 g Sepharose). In a typical preparation, 70 μg pure antibodies were recovered from 700 μl serum, representing 1% of the initial protein amount. Concentrated antibodies were stored in PBS with 30% glycerol at −20°C.

Protein Determinations and Gel Electrophoresis

All protein fractions were denatured by heating at 100°C for 3 min in electrophoresis sample buffer (Laemmli, 1970). When dilute, supernatant fractions were first precipitated by the addition of 8 vol cold acetone. Aliquots from the fractions dissolved in sample buffer were precipitated with acetone and dissolved in 2% SDS before protein determination (carried out according to Lowry et al., 1951).

Fractions were analyzed, according to Laemmli (1970), on SDS–polyacrylamide slab gels made with a linear 7.5–15% acrylamide gradient. Gels were stained with 0.1% Coomassie brilliant blue.

Immunoblotting

An extract of PtK_2 cells (2×10^6 cells containing ~2 mg protein) was prepared by heating cells for 5 min at 100°C in electrophoresis sample buffer in the presence of 40 μg/ml leupeptin and 2 mM PMSF. After electrophoresis and electrophoretic transfer (Towbin et al., 1979), nitrocellulose sheets were incubated in PBS, 3% BSA, for 1 h at 37°C; washed with PBS, 0.3% BSA, 0.1% Tween (wash buffer); overlaid with anti-*Paramecium* axonemal tubulin serum (1:200) or with a monoclonal anti-α-tubulin antibody (Amersham International Corp., Lesulis, France) (1:500) in wash buffer for 1 h at 37°C; washed; incubated with peroxidase-labeled goat anti-rabbit or goat anti-mouse IgG antibody (Diagnostics Pasteur, Marnes-La-Coquette, France) (1:200) for 1 h at 37°C; and washed again. The reaction was developed with 4-chloro-l-naphthol (Hawkes et al., 1982).

Microinjection

PtK_2 cells were grown on glass coverslips on which circular areas with a diameter of 1–2 mm were marked with a diamond pencil. The culture medium was buffered with 20 mM Hepes. Cells were observed with an inverted microscope (Nikon-Diaphot, Cetec Inc, Brussels, Belgium) the stage of which was held at 37°C by an air-stream incubator. Interphase and mitotic cells were identified within the circular areas and microinjected with ciliary tubulin from *Paramecium* (0.15–0.6 mg/ml in glutamate buffer); these cells could later be located by the presence of specific staining. Microinjection was performed as described by Ansorge (1982) using micropipettes drawn to a tip diameter of 0.5–1.0 μm.

Immunocytochemistry

At appropriate intervals after microinjection, the coverslips were removed from the microscopic stage, and processed at room temperature. The cells were permeabilized and fixed according to the following method. Cells were treated for 1 min with a mixture of 0.5% Triton X-100 and 0.5% glutaraldehyde in buffer 1 (Hank's buffer with 5 mM Pipes, 2 mM EGTA, 2 mM $MgCl_2$, pH 6). The cells were further fixed with 0.5% glutaraldehyde for 10 min, rinsed, and reextracted with 0.5% Triton X-100 for 30 min. The preparations were then treated with sodiumborohydride (1 mg/ml) for 15 min. All solutions up to this point were made in buffer 1.

For immunocytochemical staining, the following operations were carried out in TBS (20 mM Tris-HCl, 150 mM NaCl, pH 7.4). The preparations were rinsed, preincubated with normal goat serum (Nordic Immunological Laboratories, Tilburg, The Netherlands) (1:20, 30 min), and incubated for 1 h with the specific rabbit antibody against ciliary tubulin from *Paramecium* (0.5 μg/ml in TBS plus 1% normal goat serum). After rinsing, the cells were incubated with fluorescein-conjugated goat anti-rabbit IgG (Nordic Immunological Laboratories) (1:40 in TBS, pH 7.4, 1 h) for immunofluorescence or with goat anti-rabbit IgG coupled to 10-nm colloidal gold (Janssen Life Science Products, Olen, Belgium) (1:2 in TBS, pH 8.2, 3 h) for immunogold labeling. For double-label immunofluorescence, cells were incubated with a mixture of rabbit anticiliary tubulin (0.5 μg/ml, 1 h) and a rat monoclonal antitubulin (YL 1/2, Kilmartin et al., 1982) (1:500, 1 h), and then with a mixture of fluorescein-conjugated goat anti-rabbit IgG and rhodamine-conjugated goat anti-rat IgG antibodies (Nordic Immunological Laboratories) (1:40, 1 h). After washing, the preparations were mounted for immunofluorescence in gelvatol (polyvinyl alcohol, grade 20–30, Monsanto Polymers and Petrochemicals Co., St. Louis, MO) supplemented with 1,4-diazobicyclo-(2,2,2)octane (100 mg/ml), examined with a Nikon epifluorescence microscope and photographed on Fujichrome 400 films.

For Nanovid microscopy (De Brabander et al., 1986*b*), cells were postfixed with 1% glutaraldehyde for 10 min and mounted in gelvatol or buffer. The cells were first viewed extensively using the Hamamatsu C1966 image processing system and recorded on tape.

Electron Microscopy

Those cells which showed a normal morphology and qualitatively acceptable label in Nanovid microscopy were further processed for electron microscopy. Selected cells were treated with 2% osmium tetroxide for 1 h at 4°C. Then they were impregnated at 4°C for 1 h with 0.5% uranyl acetate supplemented with 1% phosphotungstic acid. After dehydration in a graded series of ethanol, they were embedded in Epon. Ultrathin sections were observed in a Philips Electronic Instruments, Inc. (Eindhoven, The Netherlands) EM 410 electron microscope.

Results

Preparation and Characterization of Paramecium Axonemal Tubulin and Specific Antibodies

Paramecium ciliary axonemes constitute a subcellular fraction highly enriched in tubulin which can be isolated by selective detachment of cilia from cell bodies. However, given the stability of the axonemal structure, this tubulin cannot be recovered by temperature-dependent MT depolymerization, as is the case for cytoplasmic tubulin. We therefore had to resort to a mechanical treatment. The purification steps were followed electrophoretically (Fig. 1, lanes *a–g*).

Deciliation was induced by $MnCl_2$. Tubulin (55 kD), dynein polypeptides (~300 kD), and the surface immobilization antigen (~250 kD) represent the major protein components of the cilia (Fig. 1, lanes *a* and *b*).

Demembranation of the ciliary fraction by means of 1%

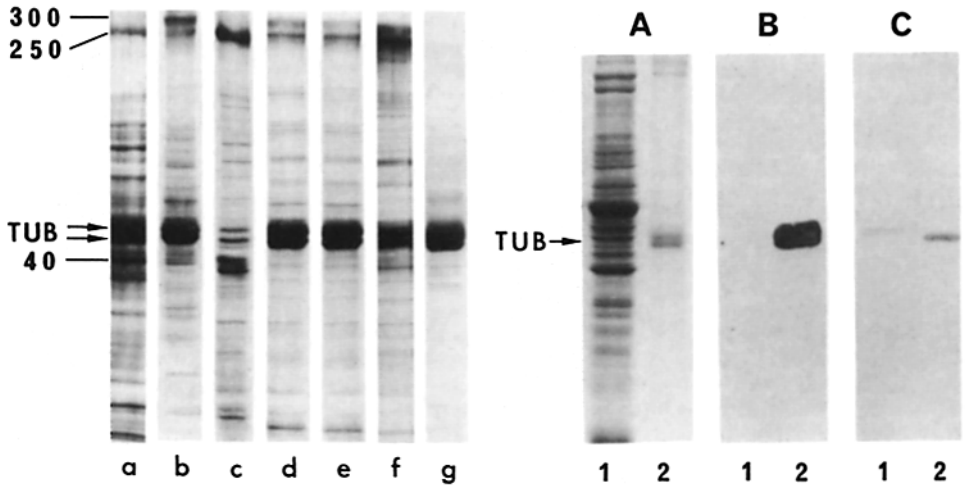

Figure 1. (*Lanes a–g*) Purification of *Paramecium* axonal tubulin, visualized after SDS-PAGE. (Lane *a*) Ciliary suspension (40 μg); (lane *b*) ciliary pellet (30 μg); (lane *c*) Triton X-100–extracted ciliary membranes (20 μg); axonemal pellet (12 μg) before (lane *d*) and after (lane *e*) dialysis at low ionic strength; (lane *f*) supernatant (20 μg) resulting from low ionic strength dialysis and subsequent centrifugation of axonemal pellet; (lane *g*) supernatant resulting from sonication of doublet MT–enriched pellet, purified tubulin (7.5 μg). The arrows on the left show the position of the tubulin bands (*TUB*); the relative molecular masses, $M_r \times 10^{-3}$, of the main components of the fractions are also indicated. Starting from a 15-liter *Paramecium* cell suspension, representing 6 ± 2 ml packed cells and ~600 mg total protein, the following protein amounts are recovered in the different fractions: ciliary pellet, 7 ± 5 mg; axonemal pellet, 5 ± 4 mg; doublet MT pellet, 3 ± 2 mg; pure tubulin, 0.6 ± 0.2 mg (values represent means ± SEM obtained for 6–20 determinations from 14 different preparations). (*A–C*) Immunological reactivity of antiaxonemal tubulin antibodies toward PtK_2 and *Paramecium* tubulins. Lanes *1*, PtK_2 cell extract (80 μg); lanes 2, *Paramecium* ciliary pellet (10 μg). (*A*) Coomassie blue–stained gel. The arrow indicates the position of tubulin (*TUB*). (*B* and *C*) Nitrocellulose filters. Both filters were first incubated either with the anti-*Paramecium* tubulin antiserum (*B*) or with a monoclonal anti-α-tubulin (*C*), and then with a peroxidase-labeled goat anti-rabbit (*B*) or goat anti-mouse (*C*) IgG antibody. The reaction was developed with 4-chloro-1-naphthol (further revelation with diaminobenzidine gave a similar pattern). Note the total lack of reactivity of anti-*Paramecium* ciliary tubulin antibodies toward PtK_2 cytoplasmic tubulin. The faster migration of the *Paramecium* α-tubulin band with respect to the mammalian α-tubulin has been previously described (Adoutte et al., 1985).

Triton X-100 selectively extracted ciliary membrane proteins, particularly the surface antigen and 40-kD polypeptides (Fig. 1, lane *c*) in agreement with previous results (Adoutte et al., 1980). The amount of Triton-extracted tubulin was minimal after low ionic strength extraction and never exceeded a few percent of the total protein amount. The axonemal pellet (Fig. 1, lane *d*) was recovered with a similar yield as in the more elaborate procedure of Adoutte et al. (1980).

When the axonemal pellet was dialyzed against a low ionic strength buffer, it was essentially freed from dynein, other solubilized MT-associated proteins, and some tubulin, (Fig. 1, lanes *e* and *f*). Negative staining and observation in the electron microscope confirmed the dissociation of axonemes into MT doublets (not shown).

Sonication of the MT doublet–enriched pellet further dissociated remaining axonemes and doublet MTs into short MT ribbons and singlet MTs (not shown). Only 20–25% of the protein was solubilized by sonication; however, it consisted of at least 80% pure tubulin (Fig. 1, lane *g*), representing 1% of the total cell protein. The low solubilization yield of *Paramecium* axonemal tubulin balanced by its good purity grade is comparable to results obtained after sonication of other axonemal tubulins (Kuriyama, 1976; Binder and Rosenbaum, 1978; Farrell and Wilson, 1978).

The functionality of purified *Paramecium* axonemal tubulin was demonstrated by its ability to assemble into single MTs (not shown) after incubation at 37°C, in a concentration range of 0.5–2.0 mg/ml, in a MT assembly buffer containing 0.15 M KCl, according to Farrell et al. (1979). Given a proportion of at least 80% tubulin in the preparation, we may infer a critical tubulin concentration <0.4 mg/ml, a value somewhat lower than those reported for other sonication-solubilized tubulin preparations (Binder and Rosenbaum, 1978; Farrell et al., 1979).

The characterization of anti-*Paramecium* ciliary tubulin antibodies has been previously described (Cohen et al., 1982; Adoutte et al., 1984, 1985; Cohen and Beisson, 1988). They display a narrow species specificity, reacting with tubulins from a limited subset of protists, whereas failing to recognize the cytoplasmic tubulins of all the metazoans tested (Adoutte et al., 1985). We have confirmed, using immunoblotting (Fig. 1, *A–C*) and immunofluorescence (Fig. 2), that they do not react with tubulin of PtK_2 cells.

Finally, coassembly of pure *Paramecium* and brain tubulins (3 and 5 μM, respectively) onto brain MT seeds was demonstrated. Whereas an antibrain tubulin antibody decorated the whole MT length, the antiaxonemal tubulin antibodies (described above) recognized only the terminal MT stretches, leaving the brain seeds (2–5 μm length) unlabeled (not shown).

Incorporation of Microinjected Tubulin in Interphase Cells

Interphase cells were microinjected and fixed at different time intervals between 0 and 30 min. Light microscopic observations were carried out after processing for immunofluorescence or Nanovid microscopy. After labeling with anti-*Paramecium* axonemal tubulin antibody, at short times (15–120 s), short MT pieces were seen all over the cytoplasm. Using double-label immunofluorescence, many short segments, appearing early after injection, could be identified as the ends of existing MTs (Fig. 2, *a* and *b*). For a number

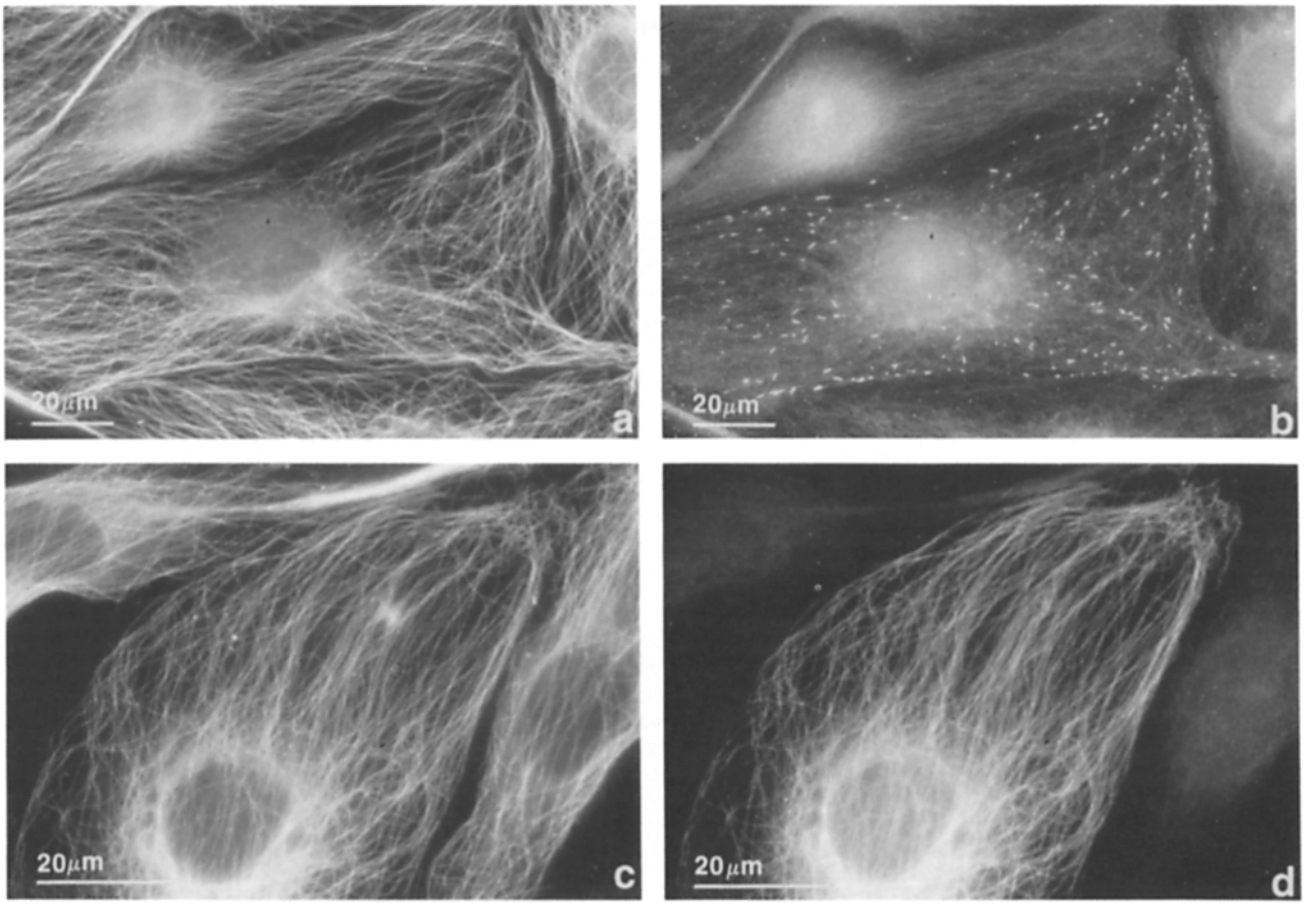

Figure 2. Double-label immunofluorescence of *Paramecium* tubulin–injected interphase PtK_2 cells. (*a* and *c*) Rhodamine antitubulin staining (YL 1/2), showing the total MT network. (*b*) Fluorescein antitubulin staining (*Paramecium* antitubulin) of the same cell as in *a*, showing MT segments distributed all over the cell. These segments can be identified mainly as the ends of existing MTs (compare *a* and *b*). The cell was fixed 30 s after injection. (*d*) Fluorescein antitubulin staining (*Paramecium* antitubulin) of the same cell as in *c*, showing a complete MT network representing a complete turnover of the MT system after injection. The cell was fixed 15 min after injection.

of other segments, this was not so clear. Thus, other possibilities, such as spontaneous polymerization or breaking and annealing cannot be excluded. Starting at 30 s–1 min, we also found short segments in the centrosome region, which probably represent nucleation of new MTs from the centrosome. The length of labeled MTs increased with time. Between 3 and 12 min, long MTs emanating from the centrosomes and directed towards the periphery and also short MT pieces were observed. After ~15–30 min, the majority of MTs became completely labeled, as observed in Fig. 2, *c* and *d*, by comparing the total tubulin immunofluorescence pattern with that of *Paramecium* tubulin. An entire MT network thus became apparent.

Ultrastructural observations (data not shown) confirmed the light microscopic data. At short times after injection, labeled MT segments were seen as the continuation of unlabeled MTs throughout the cytoplasm as well as in the vicinity of the centrosome. The labeled segments were always located distally with respect to the centrosome, suggesting that they result from elongation of previously nucleated MTs. With time, an increasing number of centrosome-attached MTs appeared that were fully labeled. These represent MTs that have been nucleated at the centrosome after microinjection of the *Paramecium* tubulin.

These results are comparable to those obtained after microinjection of fluorescein-labeled tubulin (Soltys and Borisy, 1985) and of biotin-labeled tubulin (Schulze and Kirschner, 1986) into interphase fibroblasts; they show both elongation of existing MTs and new MT nucleation at the centrosome.

To obtain an idea about the MT assembly rate, frames of immunogold-labeled cells observed with Nanovid microscopy were stored on a computer for MT segment length measurement and statistical analysis. Cells fixed between 1 and 6 min after microinjection were analyzed, and the resulting polymerization rate was 2.6 μm/min, with extreme values of 1.2 and 5.5 μm/min (Fig. 3).

Incorporation of Microinjected Tubulin in Mitotic Cells

Our major objective was to investigate the sites of MT assembly during the early stages of spindle assembly. In particular, we wanted to determine at which stage tubulin incorporation is seen at the kinetochores and whether this occurs before kinetochore fibers have been formed.

In a first series of experiments, cells at different stages from prophase to metaphase were injected with *Paramecium* tubulin and followed with time-lapse, phase-contrast micros-

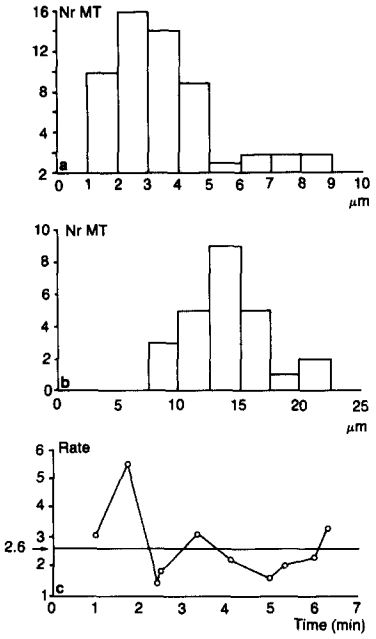

Figure 3. Length distribution of labeled MT segments. PtK_2 interphase cells were fixed 1 (*a*) and 6 min (*b*) after microinjection (MT numbers [*Nr MT*] vs. labeled MT segment lengths [μm]). After 1 min, the majority of labeled MT segments have lengths between 1 and 5 μm with extreme values of 1 and 9 μm. After 6 min, the majority of labeled MT segments have lengths between 10 and 17 μm with extreme values of 7 and 22 μm. The increase in mean length as a function of time gives an indication for the polymerization rate (μm/min), which is represented in *c* for different cells fixed between 1 and 6 min after injection.

copy. All the cells completed mitosis normally and within the usual time range. Mitotic cells at different stages from prophase to metaphase were then microinjected and fixed after increasing time intervals ranging from 30 s to 6 min. They were processed either for immunofluorescence, or for immunogold labeling and observation with video-enhanced contrast microscopy (De Brabander et al., 1986*b*). The latter approach proved to have several important advantages. In the bright-field mode, the distribution of labeled MT segments could be recorded at high magnification and resolution, and extensively followed in subsequent optical sections without any time limit imposed by fading. Because the contrast can be adjusted at will, detailed information could be obtained not only in peripheral regions but also in areas where the MT density usually blurs the image obtained with immunofluorescence, except when confocal laser scanning is used (White et al., 1987). By switching to video-enhanced, differential-interference contrast microscopy, the relationship between the location of the labeled MT portions, the mitotic poles, and the chromosomes could be established accurately. Optimal settings could be chosen which allowed simultaneous visualization of subcellular structures and gold label.

These experiments showed that, up to 1–2 min after microinjection, endwise elongation of aster MTs as well as incorporation at the centrosomes and the kinetochores could be distinguished (Fig. 4). When the cells were fixed after longer time intervals, the mitotic spindle was virtually entirely labeled. The lengths of labeled segments of aster MTs and the label intensity at the centrosomes in cells injected at prophase, prometaphase, or metaphase, and fixed at short times after microinjection, were greater than those observed in cells injected in interphase and fixed at the same times, indicating a faster MT turnover and a greater nucleation capacity of the centrosomes in mitotic than in interphase cells, in agreement with other studies (Mitchison et al., 1986; Schulze and Kirschner, 1986).

Cells injected at prophase when the nuclear membrane is still intact and fixed within 1 min showed a very dense incorporation at the centrosome, probably representing new nucleation (Fig. 4, *a* and *b*). The label density was usually similar at the two poles. Endwise elongation of aster MTs close to the centrosomes as well as elongation of remaining cytoplasmic MTs in the periphery were consistently observed. No assembly was seen within the nuclear compartment as long as the nuclear membrane remained intact.

In the cells injected at metaphase, when the chromosomes had congressed at the equator, nucleation of MTs at the centrosomes as well as endwise elongation of aster MTs was observed. In addition, however, short, relatively thick, labeled segments were associated in a bipolar fashion with the centromere regions of all chromosomes (Fig. 4, *g* and *h*). Ultrastructural observations (not shown) confirmed that these labeled segments were located at the kinetochore-associated ends of kinetochore fiber MTs the major portion of which, directed towards the poles, was unlabeled. We could thus confirm the ultrastructural observations described in metaphase cells (Mitchison, 1985; Mitchison et al., 1986).

The organization of the metaphase spindle is rather uniform and all kinetochores are known to be attached to a kinetochore fiber. Moreover, it is relatively easy to section metaphase cells parallel to the longitudinal axis and to obtain sufficient numbers of sections in which kinetochore MTs can be followed over long distances towards the pole. In contrast, during prometaphase, the distribution of the chromosomes and their relationship with the centrosomes is extremely variable and complex. Kinetochore fibers appear asynchronously and unipolar associations are frequent. To investigate this complex situation, we adopted a combined light microscopic and ultrastructural approach. Cells were injected at different stages of prometaphase, as judged by the distribution of the chromosomes. They were fixed after 1 min and processed for immunogold labeling. The coverslips were mounted on slides and extensively observed and recorded on tape in thorough focus series with video contrast-enhancement microscopy. They were then further processed for serial section EM. This allowed us to locate individual chromosomes in relation to the centrosomes, kinetochore fibers, and labeled MT segments in whole cells, which was of great help in the interpretation of the subsequent ultrastructural data.

Throughout prometaphase, the incorporation of tubulin in aster MTs was similar to that previously observed at metaphase (Mitchison, 1985; Mitchison et al., 1986). At the centrosomes, unlabeled MTs were present among many newly nucleated fully labeled ones (Figs. 5–8). Peripheral elongation of unlabeled MTs was frequently observed (Fig. 8).

We injected five cells at very early prometaphase when the nuclear membrane had already disappeared but in which most chromosomes were at a distant location from the centrosomes. These had not yet been separated in most cells.

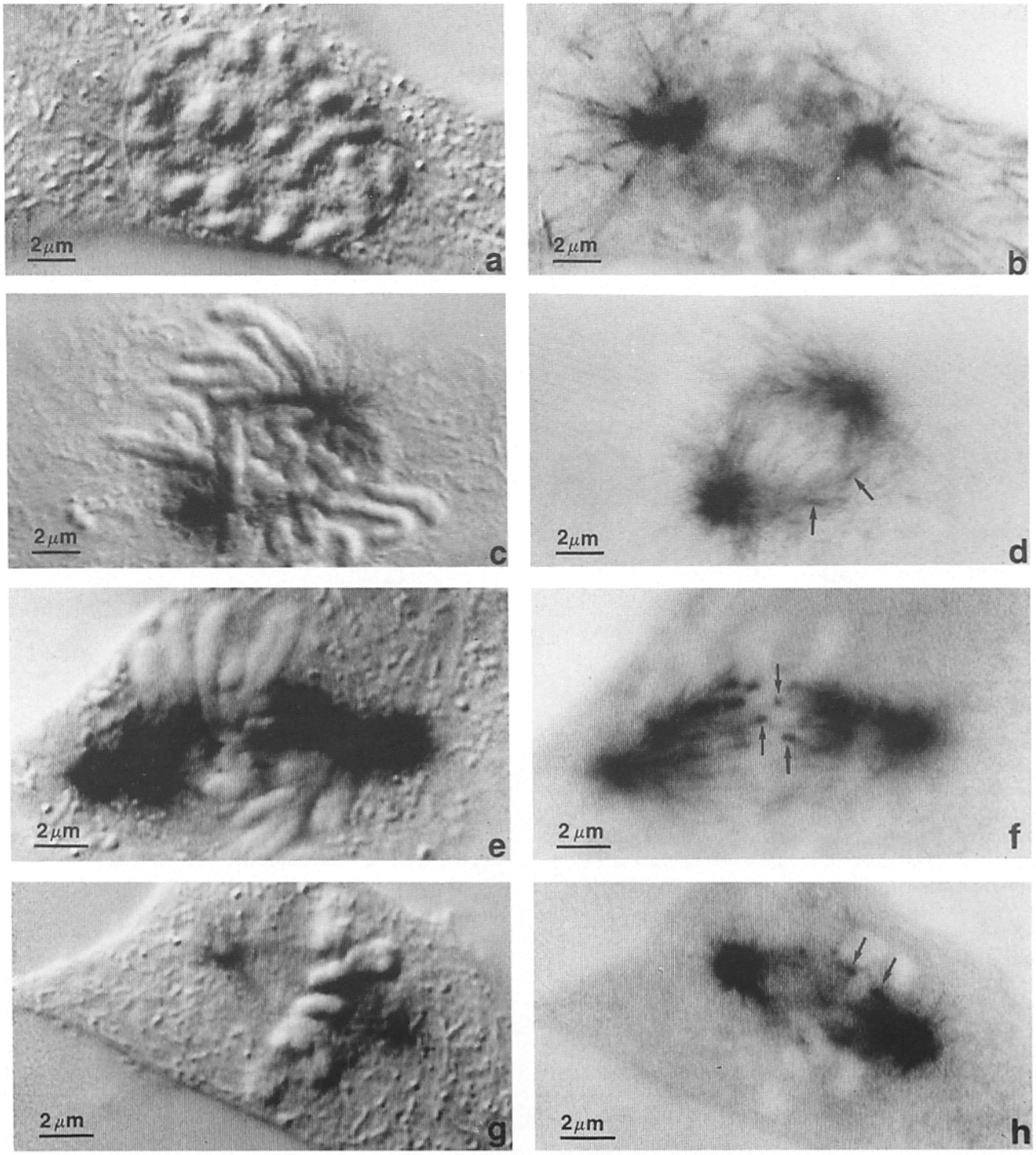

Figure 4. Immunogold labeling of mitotic cells. Mitotic PtK_2 cells were microinjected with *Paramecium* tubulin, fixed 1 min after microinjection, and stained with specific *Paramecium* antitubulin and a secondary antibody coupled to colloidal gold. Cells were viewed with video microscopy using differential-interference contrast (*a*, *c*, *e*, and *g*) and bright-field observation (*b*, *d*, *f*, and *h*). (*a* and *b*) Prophase. Incorporation is most prominent in the dense pericentrosomal asters. MT segments can also be seen in the peripheral cytoplasm. No incorporation is seen within the nuclear domain. (*c* and *d*) Early prometaphase. Note the incorporation in the dense polar asters and in the interzonal MTs. Short stretches of incorporation at kinetochores are denoted by arrows. (*e* and *f*) Late prometaphase. Incorporation is seen at the poles, in some interzonal MTs, and very prominently at the kinetochore-associated ends of kinetochore fibers (*arrows*). (*g* and *h*) Metaphase. Incorporation is still most prominent at the poles and at the kinetochores (*arrows*).

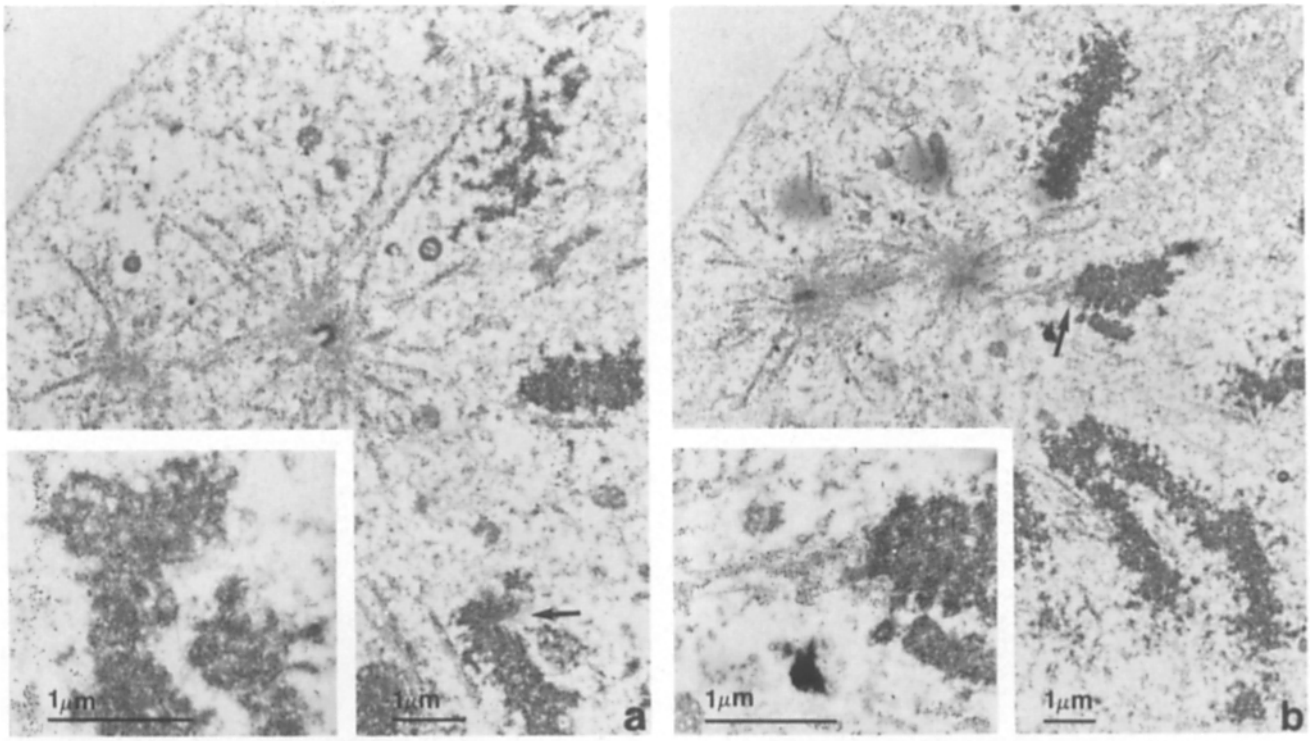

Figure 5. Ultrastructural localization of *Paramecium* tubulin in an early (monopolar) prometaphase cell fixed 1 min after microinjection. Serial sections are shown in *a* and *b*. The centrosomes are surrounded by many labeled MTs. The insets show the kinetochore regions denoted by the arrows. The kinetochore in *a*, facing away from the centrosomes, has no MT associated with it. The kinetochore in *b*, facing a centrosome, is attached to short kinetochore MTs that have incorporated *Paramecium* tubulin.

Kinetochore bundles could not be discerned in these cells. We were unable to detect any discrete incorporation at the kinetochores in these cells using video-enhanced contrast microscopy. Four cells were studied at the ultrastructural level. Out of 17 kinetochores that could be recognized, three were located close to a centrosome and connected to a short kinetochore fiber. The kinetochore-associated ends of these MTs had clearly incorporated injected tubulin while the poleward segment was free of label (Fig. 5 *b*). Other kinetochores located further away from the centrosomes or facing away from the center of the monopolar aster (Fig. 5 *a*) were entirely free of associated MTs. In view of what is observed after nocodazole reversal (De Brabander et al., 1981), short labeled MT stubs in the vicinity of these kinetochores were specifically searched for but none were found. The morphology of these MT-free kinetochores (Fig. 5 *a*) was strikingly similar to what is seen in cells deprived of MTs with colchicine or nocodazole (Witt et al., 1980; De Brabander et al., 1981). They consist of a chromatin-associated dense plate and an outer fuzzy corona.

We injected 18 cells at further stages of prometaphase progression, in which the chromosomes were distributed at various distances between the two poles of the bipolar or multipolar (two cells) spindle. In these cells, kinetochore fibers at various stages of formation could be discerned (Figs. 4, *d* and *f*, 6, and 7). Ten cells were fixed after 1 min. In nine of them, we could detect discrete kinetochore-associated tubulin incorporation with Nanovid microscopy (Figs. 4, 6, and 7). Eight microinjected cells were fixed after 2–5 min. In seven, kinetochore-associated incorporation was seen. The extent of kinetochore-associated incorporation (numbers of labeled kinetochores and density of the labeled stubs) was clearly related to the progression towards metaphase (compare Figs. 4, *c* and *d*, and 6, *a* and *b*, with Fig. 7, *a–c*). Six cells fixed after 1 min could be evaluated ultrastructurally. Out of 41 kinetochores examined, 25 were attached to a kinetochore fiber. These were unlabeled along most of their length except for a short labeled segment which was present at all 25 kinetochores (Figs. 6 and 7). Similarly to the observations made during metaphase (Mitchison et al., 1986), the length of labeled MT segments varied slightly for different kinetochore fibers in the same cell whereas it was quite homogenous for the MTs in a single kinetochore fiber (Figs. 6 and 7). This explains the prominent visibility of the kinetochore-associated incorporation with Nanovid microscopy (Figs. 4 *f*, 6 *b*, and 7, *a–e*). Labeled MT segments at the kinetochore were always shorter than labeled aster MTs (Figs. 6 and 7). In cells fixed after longer incubation times, labeled segments grew longer (Fig. 8), as is also observed during metaphase (Mitchison et al., 1986). This made it more difficult to trace individual MTs to the point where they became unlabeled, and to discern the labeled stretches with Nanovid microscopy. The prominence of unlabeled MT segments in the poleward portion of the kinetochore fibers, while most aster MTs and interzonal MTs are labeled after 5 min, confirm that, during prometaphase as well as in metaphase (Mitchison et al., 1986), kinetochore MTs apparently have a slower assembly rate than aster or interzonal MTs.

Incorporation of tubulin was seen at both sister kinetochores whenever amphitelic attachment to both opposite kinetochore fibers was established (Figs. 4, *e* and *f*, and 7).

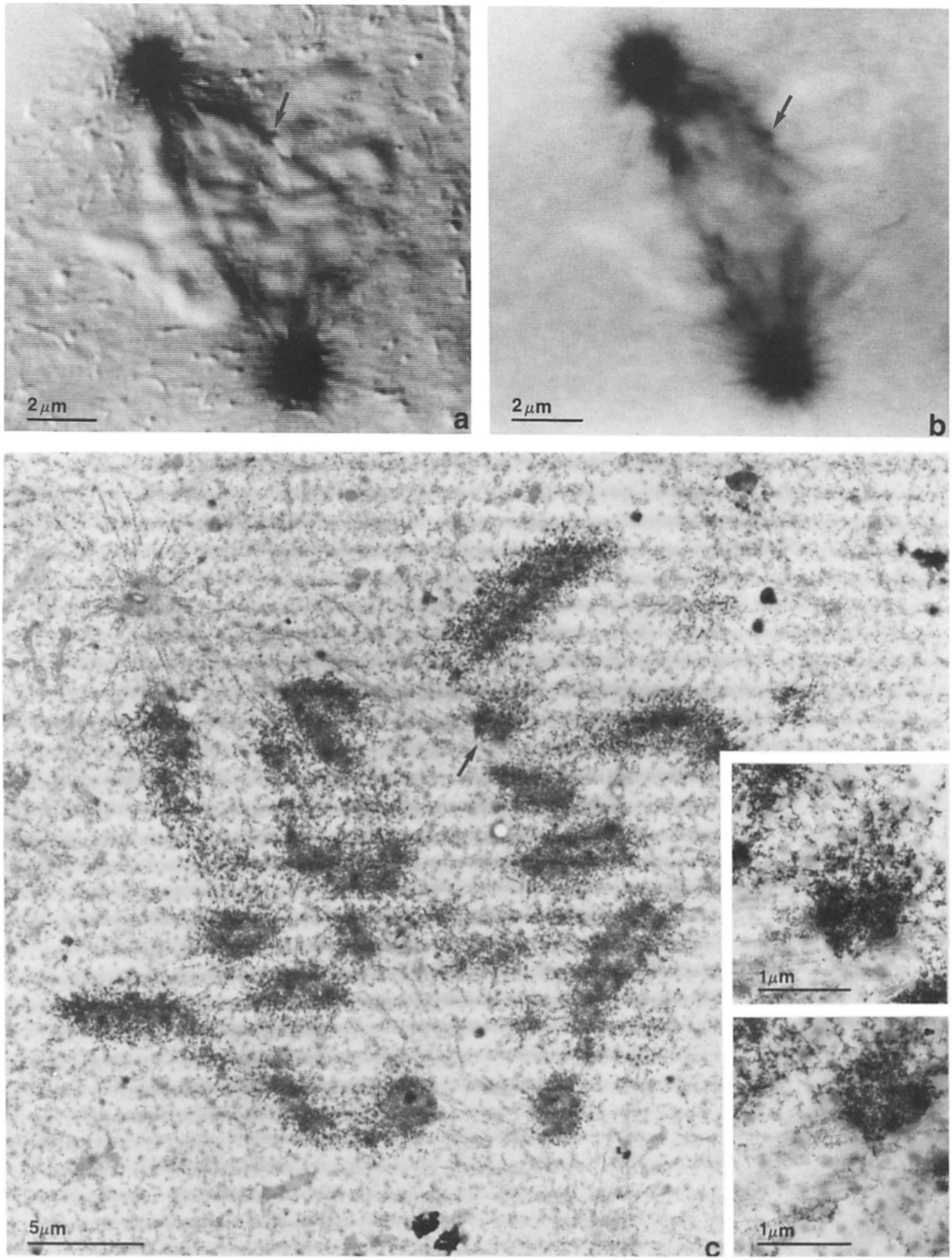

Figure 6. Light microscopic and ultrastructural localization of *Paramecium* tubulin in an early bipolar prometaphase cell fixed 1 min after microinjection. (*a*) Differential-interference contrast. (*b*) Bright field. (*c*) Ultrastructural overview. Many labeled aster MTs are seen as well as kinetochore-associated labeled segments. Note that within the kinetochore fiber (e.g., of the chromosome marked with an arrow in *c*), newly incorporated tubulin is confined to the pole area and to the kinetochore-associated ends. The centromere region depicted by the arrows in *a–c* is shown at higher magnification in two serial sections in the insets. The kinetochore facing the upper pole is attached to MTs that show incorporation at the kinetochore-associated ends. No MTs are seen at the opposite sister kinetochore.

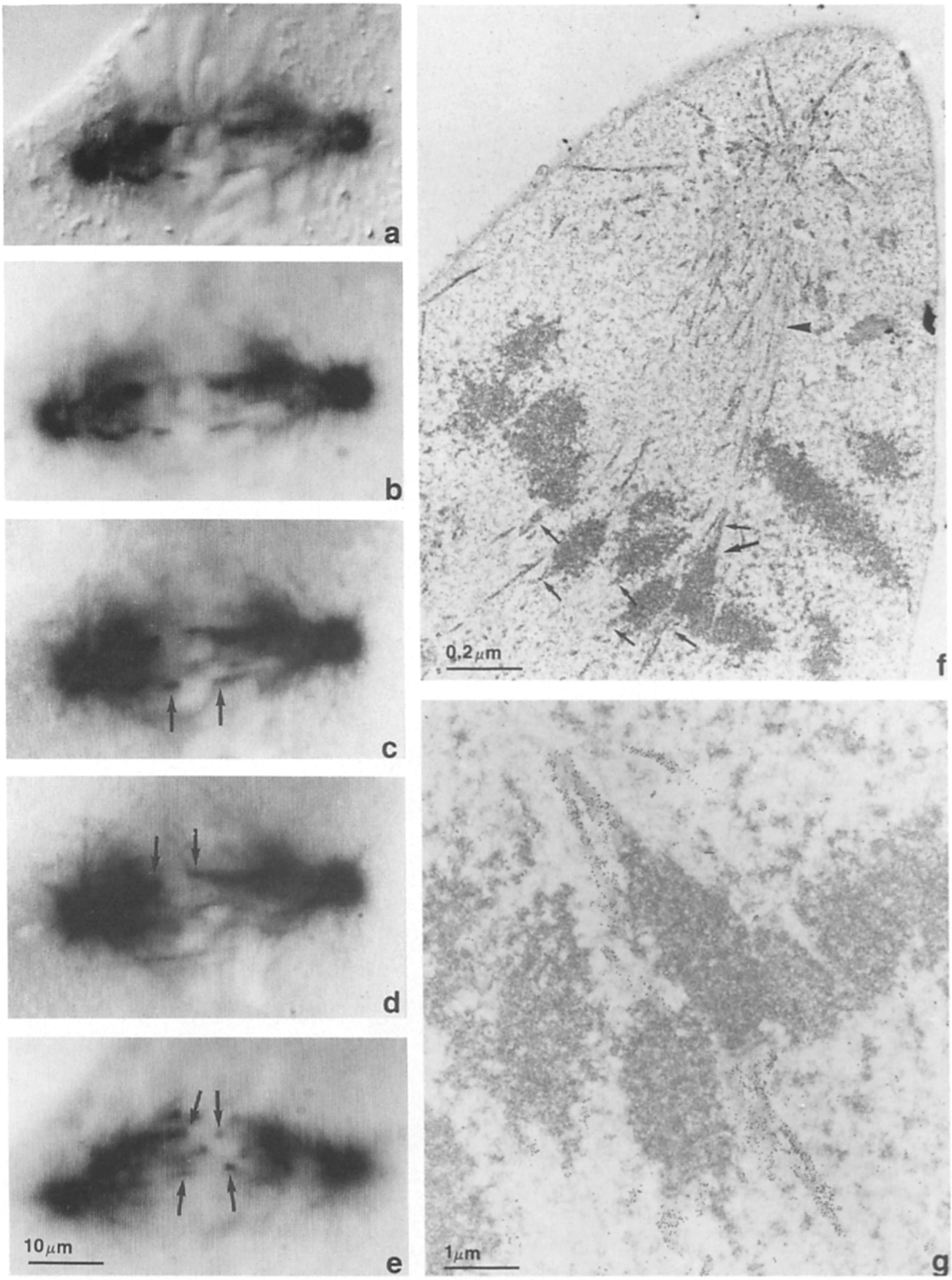

Figure 7. Light microscopic and ultrastructural localization of *Paramecium* tubulin in a late bipolar prometaphase cell fixed 1 min after microinjection. (*a*) Differential-interference contrast. (*b–e*) Bright-field images at different focal planes showing extensive incorporation at sister kinetochores (*arrows*). *a*, *b*, and *e* have been taken at a low contrast setting to show kinetochore-associated incorporation more clearly. (*f*) Ultrastructural overview of the left half-spindle. Aster MTs are labeled. Within the half-spindle, unlabeled MTs and many labeled segments are seen (*arrowhead*). The latter probably represent elongation of pole MTs. Several kinetochores attached to labeled MT segments are denoted by arrows. (*g*) Higher magnification of the chromosome denoted by a large arrow in *f*. The two sister kinetochores are associated with labeled MT segments.

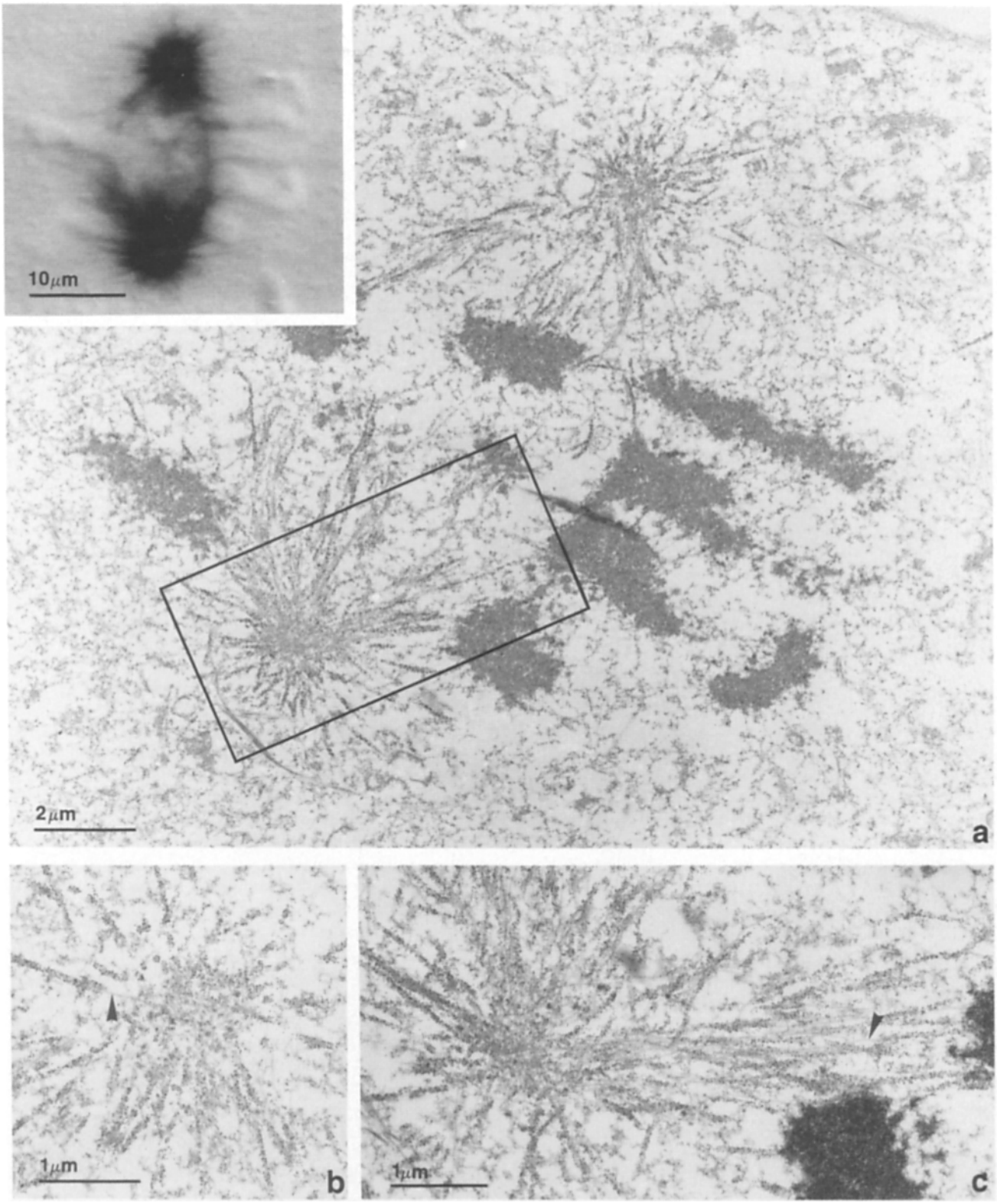

Figure 8. Ultrastructural and light microscopic localization of *Paramecium* tubulin in a prometaphase cell fixed 5 min after microinjection. (*a*) Ultrastructural overview. The inset shows the Nanovid image of the same cell. (*b*) Higher magnification of an aster showing endwise elongation of the MT marked with an arrowhead. (*c*) Higher magnification of a kinetochore fiber (adjacent section to the region framed in *a*). Note that the majority of the aster MTs are labeled along most of their length, suggesting rapid renewal. Within the kinetochore fibers, many long stretches of unlabeled MTs remain. These are probably the MTs that have become stabilized by association with a kinetochore. The arrowhead in *c* marks the transition between the labeled, kinetochore-associated portion and the unlabeled, poleward portion of a kinetochore MT. Note also that along the entire length of the kinetochore fiber, labeled MT stretches are present which preclude the visualization of separate kinetochore-associated incorporation at the light microscopic level (compare with Figs. 6 and 7).

The length of the opposite labeled stretches associated to each sister kinetochore varied considerably. However, we could not establish any consistent relationship between the relative distance of the chromosomes from the opposite spindle poles and the respective length of the labeled stretches.

16 of the 41 kinetochores examined did not show any associated tubulin incorporation. These were usually found in midprometaphase cells (Fig. 6) when many chromosomes were as yet attached to only one kinetochore fiber. In favorable sections, incorporation was seen at the anchored kinetochore while the sister kinetochore, facing away from the centrosome, was free of MTs (Fig. 6). As was the case during early prometaphase, the MT-free kinetochores showed the same morphology as colchicine-treated kinetochores. It should be stressed that we never saw short labeled MT stubs in the vicinity of these kinetochores that were not yet attached to a kinetochore fiber. Neither did we see any kinetochore that was attached to unlabeled MTs or unlabeled MTs that became labeled at a distance from the kinetochore.

The observations thus show that, during prometaphase, independent nucleation of MTs in the vicinity of the kinetochores does not occur or is at least an extremely infrequent event. Instead, sets of MTs constantly nucleated at the centrosomes apparently become anchored to kinetochores. Since the length of labeled MT segments at the kinetochores is identical within a given kinetochore fiber, it appears that simultaneous attachment of several MTs to one kinetochore would occur, followed by subunit incorporation at a similar rate within these MTs at the kinetochore attached ends.

Discussion

The present work shows that microinjected *Paramecium* tubulin is efficiently incorporated into existing MT complexes of PtK_2 cells. This has allowed us to confirm previous observations on MT dynamics in fibroblasts during interphase and mitosis (Soltys and Borisy, 1985; Mitchison et al., 1986; Schulze and Kirschner, 1986). Confirmation of these data with an independent approach is of interest since our techniques differ from those used previously in several ways.

First, we have used chemically unmodified tubulin. The validity of our strategy consisting in microinjection of *Paramecium* tubulin in a vertebrate cell, in order to determine where tubulin subunits are incorporated into MTs, depends on how accurately *Paramecium* tubulin incorporation mimics the behavior of endogenous tubulin subunits. We have shown that, even at an equimolar ratio of *Paramecium* to hog brain tubulin, efficient coassembly occurs in vitro. Based on the assumption that the injection volume is 10% of the cell volume and that the total endogenous concentration of tubulin is 2 mg/ml (Hiller and Weber, 1978), of which 50% is polymerized, Schulze and Kirschner (1986) estimated that microinjection of a solution containing 0.5 mg/ml tubulin would increase the total tubulin concentration by only 2.5%; in fact, injection of up to 20-fold higher concentrations did not perturb the measured elongation rate (~3.6 μm/min). Therefore, we expect that microinjection of 0.15–0.6 mg/ml *Paramecium* tubulin does not disturb the MT steady-state dynamics. This is reflected by the fact that we find a roughly similar elongation rate (~2.6 μm/min), although we used a different cell type.

We can also estimate the sensitivity of our detection system for incorporation of *Paramecium* tubulin. The lowest injected concentration which was still able to produce a virtually complete image of the MT system was 0.15 mg/ml. Assuming that the *Paramecium* and PtK_2 tubulins incorporate equally into MTs, ~1 in every 133 subunits should be of *Paramecium* origin. If there are ~1,600 subunits/μm, then ~12 subunits/μm, each probably marked with several secondary labeled antibodies, are visible as a linear structure. This is in the same range as the detection threshold estimated for dichlorotriazinylaminofluorescein-labeled tubulin (Soltys and Borisy, 1985).

The ability of *Paramecium* tubulin to copolymerize with vertebrate tubulin in vitro is not unexpected. In fact, tubulins from very different sources such as yeast (Water and Kleinsmith, 1976), *Aspergillus* (Sheir-Neiss et al., 1976), *Tetrahymena* (Maekawa and Sakai, 1978), *Naegleria* (Lai et al., 1979), *Polytomella* (McKeithan and Rosenbaum, 1981), and *Chlamydomonas* (Weeks and Collis, 1976) copolymerize with mammalian brain tubulin in vitro. Similarly, tubulin-containing organelles such as basal bodies or flagellar axonemes of *Chlamydomonas* (Allen and Borisy, 1974) and sea urchin sperm (Binder et al., 1975) are able to nucleate brain tubulin assembly *in vitro*. More recently, a chicken–yeast chimeric β-tubulin has been incorporated *in vivo* in mouse 3T3 cells, at a high concentration (10% of the amount of endogenous tubulin), without perturbation of the microtubular structure (Bond et al., 1986), although the COOH-terminal end, from yeast, contains the most highly divergent β-tubulin sequence yet identified (73% homology with vertebrate tubulin; Little et al., 1986). The first *Paramecium* α-tubulin gene sequenced (Spitzer, 1986) exhibits 86% homology with vertebrate α-tubulins. It appears, therefore, that divergence in tubulin amino acid sequence has not affected conservation of configuration essential for subunit interactions and assembly. The interconvertibility of tubulin subunits from very distant organisms correlates well with the highly conservative nature of MT architecture.

In addition to its characteristic sequence, *Paramecium* axonemal tubulin is acetylated. It would be interesting to explore whether the injected tubulin is processed by the cell (e.g., tyrosinated and deacetylated) before or after its incorporation into MTs.

A second difference with respect to previous work concerns our fixation protocol which ensures very rapid fixation without prior extraction. We can thus be confident that the images reflect as well as possible the true situation at the time of fixation. Because our observations are similar to those published before, using extraction in MT-stabilizing buffers, we can confirm that such procedures can be used reliably if they are carefully controlled.

Thirdly, the methods we have used to observe the cells have several important advantages. Nanovid immunocytochemistry (De Brabander et al., 1986*b*) allows a high resolution observation of the label distribution and easy combination with high resolution, differential-interference contrast microscopy. Most importantly, the possibility to first observe and record the three-dimensional distribution of the label in whole cells, and then to section the same cells to analyze in detail the distribution of the same label at the ultrastructural level, has proven to be extremely valuable. Accurate information can be obtained with relatively few cells, because one has to rely less on the probability to find the appropriate cells.

Our data concerning interphase PtK_2 cells largely confirm those published on fibroblasts (Soltys and Borisy, 1985; Schulze and Kirschner, 1986). The salient observations are distal assembly of MTs (i.e., at their plus ends, towards the cell periphery) together with new nucleation at the centrosome, as occurs in vitro (Mitchison and Kirschner, 1984*a*). Elongation of existing MTs occurs faster than new nucleation at the centrosome although the tubulin is actually injected in the centrosomal region, which means that *Paramecium* tubulin has rapidly diffused throughout the cell. From the overall MT growth rate of 2.6 μm/min (or 70 subunits/s), corresponding to a rate constant of $\sim 7 \times 10^6$ M^{-1}/s^{-1}, and assuming only one subunit addition on MT ends at equilibrium, one can estimate the half-time of MT turnover in the whole cell to be ~15 min, a value which roughly fits with our experimental data. Our observations confirm that the MT population is not only quickly elongating from the centrosomes to the cell periphery, but is also rapidly replaced by new MTs nucleated at the centrosome. This polymerization of new MTs implies, however, a concomitant depolymerization of other MTs, in agreement with the "dynamic instability" model (Mitchison and Kirschner, 1984*b*). Subunit exchange along the MT walls does not occur, since unlabeled MT segments coexist with labeled ones at the same time and a sharp boundary between labeled and unlabeled segments always exists in the same MT.

At all stages of mitosis, from prophase to metaphase, endwise MT assembly as well as new nucleation at the centrosomes is seen. It is striking that the rate of MT turnover is much greater in mitotic than in interphasic cells. This can best be explained by the enhanced nucleation capacity of the mitotic centrosomes, resulting in a rapid depletion of the cell in free tubulin, bringing its concentration below that of the steady-state level, thus inducing MT depolymerization and release of free tubulin, again available for MT elongation or new nucleation, as predicted by the dynamic instability model. The overall outcome is that the mitotic array displays, as a whole, an apparent structural stability, while its individual component MTs are much more dynamic than during interphase.

In the course of prometaphase and metaphase, proximal incorporation of tubulin is also seen at kinetochores bearing MTs, in agreement with the data of Mitchison et al. (1986) at metaphase. Essentially two hypotheses have been put forward to account for the formation of the kinetochore fibers, and their popularity has been swinging back and forth for many years. Detailed ultrastructural investigations (Roos, 1976) and many different experimental manipulations, in vitro as well as in vivo (reviewed by Rieder, 1982), have not solved the problem.

The first hypothesis sees the kinetochore as a nucleating and assembly-promoting structure. We and others have been advocating such an active role for the kinetochore in the construction of the kinetochore fiber. This was based on the observation that, after release from a nocodazole block, new MTs were preferentially nucleated at all kinetochores as well as at the centrosomes. A kinetochore fiber was formed on those kinetochores that were sufficiently close to a centrosome. Kinetochores that faced away from the centrosome or that had been widely separated lost the MTs that had been initially formed. We thus expected that the set of MTs emanating from the kinetochores form interdigitating MTs with the set of MTs originating at the centrosome (De Brabander, 1982; De Brabander et al., 1981, 1986*a*). This hypothesis has been criticized predominantly on the basis that the nocodazole block leads to an abnormally high concentration of free tubulin that may artificially be induced to assemble after washing out the inhibitor (Pickett-Heaps et al., 1982). Indeed, MT nucleation by the kinetochores occurs in vitro only at high tubulin concentrations, above the steady-state level (Mitchison and Kirschner, 1985*a*), and thus the kinetochores appear to be poor nucleating centers. Moreover, according to this hypothesis, by analogy with the in vitro situation (Mitchison and Kirschner, 1985*a*), kinetochore MTs of mixed polarity are expected in vivo, in contradiction with the uniform polarity of the half-spindle which displays MT minus ends at the centrosome and plus ends at the kinetochores (Euteneuer and McIntosh, 1981; Telzer and Haimo, 1981). To be compatible with the polarity of the half-spindle, kinetochore-induced nucleation and distal assembly would imply assembly at the unfavorable minus ends of MTs (Fig. 9 *A*). As for kinetochore-induced nucleation and proximal assembly, while it generates MTs of the right polarity (Fig. 9 *B*), it has never been observed in vitro. Furthermore, MT nucleation by kinetochores might imply their capture by the centrosomes, which has so far never been reported. Finally, MT nucleation by the kinetochores, followed by either distal or proximal assembly at the kinetochores, leads, after microinjection of exogenous tubulin, to specific labeling patterns of kinetochore MTs with free ends (described in Fig. 9, *A* and *B*) which we have never observed at prometaphase. Indeed, our data show that incorporation of tubulin in the vicinity of the kinetochore is not seen during prophase and early prometaphase, as long as the kinetochore is not yet connected to any pole by MTs. Incorporation occurs only into preexisting kinetochore MTs emanating from centrosomes, at all stages of prometaphase and at metaphase, and as well in monopolar as in bipolar spindles. Chromosomes that are separated or kinetochores facing away from a centrosome do not interact with any MT, which demonstrates that they do not nucleate MTs. Apparently, in undisturbed prometaphase cells, the tubulin concentration is too low for the kinetochore to induce nucleation, even when additional tubulin is injected. On the whole, although there is a remote possibility that the kinetochore becomes competent only at a rather late stage, our observations force us to reject the hypothesis we advocated.

The second hypothesis states that the chromosome is passive for MT nucleation as well as for tubulin incorporation and merely attaches to MTs growing from the poles. In connection with this, a mechanism accounting for tubulin labeling at the kinetochores, discussed by Mitchison et al. (1986), would be the capping by kinetochores of MTs emanating from the centrosomes, possibly followed by their release, partial depolymerization, repolymerization, and recapture (Fig. 9 *C*). This is however hardly compatible with the absence of unlabeled kinetochore MTs, with the lack of long labeled segments at short times after microinjection (Fig. 9 *C*), and with the uniform length of incorporation in all MTs at one kinetochore. This mechanism could not account for chromosome translocation either.

Recent in vitro (Mitchison and Kirschner, 1985*b*) and in vivo (Mitchison et al., 1986) experiments, showing incorporation of tubulin at the kinetochores, had suggested a somewhat intermediate mechanism assigning active roles, in the formation of kinetochore MTs, to centrosomes as well as to

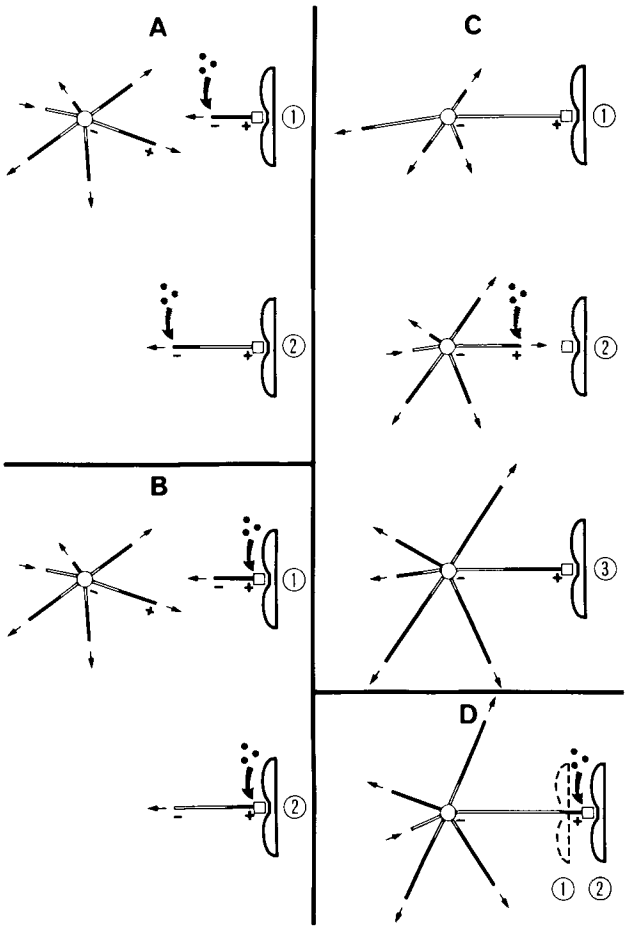

Figure 9. Possible roles for kinetochores at prometaphase. Four possible models are depicted with the predicted labeling patterns after microinjection of exogenous tubulin (*solid circles*). A half-spindle is represented with MTs at one centrosome (*open circle*) and at one chromosome with its kinetochore (*open square*). MT polarity is indicated by the minus and plus signs. MTs are either unlabeled (*open thin rectangles*), fully labeled (*solid thin rectangles*), or partially labeled. The direction of the arrows indicates whether the MTs are growing or shrinking. The curved arrows show the site of tubulin subunit incorporation into kinetochore MTs. (*A*) Nucleation and distal assembly at the kinetochore. (*1*) Nucleation after microinjection yields fully labeled kinetochore MTs; (2) elongation, after microinjection, of MTs previously nucleated at the kinetochore, yields distally labeled kinetochore MT segments. (*B*) Nucleation and proximal assembly at the kinetochore. (*1*) Nucleation after microinjection yields fully labeled kinetochore MTs; (2) proximal assembly, after microinjection, of MTs previously nucleated at the kinetochore, yields proximally labeled kinetochore MT segments. (*C*) Capture of centrosomal MTs by kinetochores without assembly, and possible release, partial disassembly, reassembly of centrosomal MTs, and recapture. (*1*) Capture before microinjection and no polymerization after capture yield unlabeled kinetochore MTs; (2) polymerization, after microinjection, of centrosomal MTs either not yet captured or released and depolymerized after capture, yield bare kinetochores; (*3*) recapture by the kinetochores of centrosomal MTs repolymerized after microinjection can yield long proximally labeled kinetochore MTs at short times after microinjection. (*D*) Capture of centrosomal MTs and proximal assembly at the kinetochores. (*1*) Capture before microinjection; (2) followed, after microinjection, by tubulin incorporation at the kinetochores, yield short, proximally labeled kinetochore MTs at short times after microinjection, and ensure chromosome translocation.

kinetochores. The centrosomes generate new MTs very rapidly, these probe the cytoplasm and eventually are captured by a kinetochore. The kinetochore then stabilizes these MTs and promotes proximal assembly and chromosome congression (Fig. 9 *D*). Thus, it is the specificity of the centrosome in nucleating MTs of uniform polarity which defines the polarity of the half spindle. An alternative mechanism consisting of nucleation and proximal assembly at the kinetochores (Fig. 9 *B*) could nevertheless have accounted for the incorporation of tubulin observed at the kinetochores at metaphase, when kinetochore MTs are already formed (Mitchison et al., 1986, and this paper). However, our data show that the pattern of incorporation of tubulin at prometaphase, and hence at metaphase, fits only with the "capture and proximal assembly" model (Fig. 9 *D*) described above. It is worth noticing that the labeled segments at the kinetochores are always shorter than the labeled astral MTs. This could either reflect the fact that the rate of MT proximal assembly at the kinetochores is much lower than that of astral MT assembly, during prometaphase (this report, and see Fig. 6 *c*) as well as at metaphase (Mitchison et al., 1986), or that "tempered instability" of MTs (Sammak et al., 1987) occurs at the kinetochores. These in vivo observations are consistent with the in vitro situation, where the rate of MT proximal assembly at kinetochores is lower than the rate of free MT plus end assembly (Mitchison and Kirschner, 1985*b*).

Mitchison et al. (1986) argued that the continuous tubulin incorporation at both kinetochores during metaphase must generate a poleward flux of subunits in the kinetochore fiber. We show here that bipolar kinetochore-associated tubulin incorporation already occurs at prometaphase, irrespective of the location of the chromosomes in the spindle. This makes it unlikely that the incorporation merely reflects elongation of MTs when a kinetochore is moving away from a spindle pole, and suggests that a poleward flux of subunits may already be generated at prometaphase. It remains enigmatic how the necessary disassembly of the poleward portion of the kinetochore MTs would be regulated.

In conclusion, our observations on the incorporation of microinjected tubulin during early stages of kinetochore fiber formation in the course of prometaphase do not show any evidence for intrinsic MT nucleation by the kinetochores. Rather they support the concept originally proposed by Mitchison et al. (1986), based essentially on data obtained at metaphase; i.e., fast probing of the cytoplasm by centrosomal MTs and grabbing of these MTs by the kinetochores followed by stabilization and further assembly.

In addition, the present work shows that the combination of *Paramecium* ciliary tubulin and its specific antibody constitute a powerful tool whose use may be generalized to the study of MT dynamics in other eukaryotic cells.

We thank Hugo Geerts for providing us the software used for quantitative analysis of MT length measurements; Colette Simon and Dr. Dominique Pantaloni for the gift of brain tubulin and MT seeds; Guy Daneels for immunoblotting and electrophoretic work; Francine Iftode for EM observations after negative staining; Kristin Donné and Cécile Couanon for typing the manuscript; Lambert Leijssen, Guy Jacobs, and Noëlle Narradon for making the photographs; and Jan De Mey for helpful suggestions and discussions. The rat monoclonal antibody (YL 1/2) against tubulin was a generous gift from Dr. J. V. Kilmartin.

This research was supported by a grant from the Institut ter Aanmoedig-

ing van Wetenschappelijk Onderzoek in Nijverheid en Landbouw (Brussels, Belgium) and by the CNRS and the Université Paris-Sud (Orsay-Cedex, France).

Received for publication 21 June 1988 and in revised form 21 November 1988.

References

Adoutte, A., M. Claisse, and J. Cance. 1984. Tubulin evolution: an electrophoretic and immunological analysis. *Origins Life.* 13:177–182.

Adoutte, A., M. Claisse, R. Maunoury, and J. Beisson. 1985. Tubulin evolution: ciliate-specific epitopes are conserved in the ciliary tubulin of metazoa. *J. Mol. Evol.* 22:220–229.

Adoutte, A., R. Ramanathan, R. M. Lewis, R. R. Dute, K. Y. Ling, C. Kung, and D. L. Nelson. 1980. Biochemical studies of the excitable membrane of *Paramecium tetraurelia*. III. Proteins of cilia and ciliary membranes. *J. Cell Biol.* 84:717–738.

Allen, C., and G. G. Borisy. 1974. Structure polarity and directional growth of microtubules of *Chlamydomonas* flagella. *J. Mol. Biol.* 90:381–402.

Ansorge, W. 1982. Improved system for capillary microinjection into living cells. *Exp. Cell Res.* 140:31–37.

Binder, L. I., and J. L. Rosenbaum. 1978. The in vitro assembly of flagellar outer doublet tubulin. *J. Cell Biol.* 79:500–515.

Binder, L. I., W. L. Dentler, and J. L. Rosenbaum. 1975. Assembly of chick brain tubulin onto flagellar microtubules from *Chlamydomonas* and sea urchin sperm. *Proc. Natl. Acad. Sci. USA.* 72:1122–1126.

Bond, J. F., J. L. Fridovich-Keil, L. Pillus, R. C. Mulligan, and F. Solomon. 1986. A chicken-yeast chimeric β-tubulin protein is incorporated into mouse microtubules in vivo. *Cell.* 44:461–468.

Cohen, J., and J. Beisson. 1988. The cytoskeleton. *In Paramecium.* H. D. Görtz, editor. Springer-Verlag, Berlin, FRG. 363–392.

Cohen, J., A. Adoutte, S. Grandchamp, L. M. Houdebine, and J. Beisson. 1982. Immunocytochemical study of microtubular structures throughout the cell cycle of *Paramecium*. *Biol. Cell.* 44:35–44.

De Brabander, M. 1982. A model for the microtubule organizing activity of the centrosomes and kinetochores in mammalian cells. *Cell Biol. Int. Rep.* 6:901–915.

De Brabander, M., G. Geuens, J. De Mey, and M. Joniau. 1981. Nucleated assembly of mitotic microtubules in living PtK_2 cells after release from nocodazole treatment. *Cell Motil.* 1:469–483.

De Brabander, M., G. Geuens, R. Nuydens, R. Willebrords, F. Aerts, and J. De Mey, with the participation of J. R. McIntosh. 1986*a*. Microtubule dynamics during the cell cycle: the effects of taxol and nocodazole on the microtubule system of PtK_2 cells at different stages of the mitotic cycle. *Int. Rev. Cytol.* 101:215–274.

De Brabander, M., R. Nuydens, G. Geuens, M. Moeremans, and J. De Mey. 1986*b*. The use of submicroscopic gold particles combined with video contrast enhancement as a simple molecular probe for the living cell. *Cell Motil. Cytoskeleton.* 6:105–113.

Euteneuer, U., and J. R. McIntosh. 1981. Structural polarity of kinetochore microtubules in PtK_1 cells. *J. Cell Biol.* 89:338–345.

Farrell, K. W., and L. Wilson. 1978. Microtubule reassembly *in vitro* of *Strongylocentrotus purpuratus* sperm tail outer doublet tubulin. *J. Mol. Biol.* 121:393–410.

Farrell, K. W., A. Morse, and L. Wilson. 1979. Characterization of the in vitro reassembly of tubulin derived from stable *Strongylocentrotus purpuratus* outer doublet microtubules. *Biochemistry.* 18:905–911.

Füller, G. M., B. R. Brinkley, and J. M. Boughter. 1975. Immunofluorescence of mitotic spindles by using monospecific antibody against bovine brain tubulin. *Science (Wash. DC).* 187:948–950.

Gorbsky, G. J., P. J. Sammak, and G. G. Borisy. 1987. Chromosomes move poleward in anaphase along stationary microtubules that coordinately disassemble from their kinetochore ends. *J. Cell Biol.* 104:9–18.

Hawkes, R., E. Niday, and J. Gordon. 1982. A dot-immunobinding assay for monoclonal and other antibodies. *Anal. Biochem.* 119:142–147.

Hill, A. M., R. Maunoury, and D. Pantaloni. 1981. Cellular distribution of the microtubule-associated proteins HMW (350 K, 300 K) by indirect immunofluorescence. *Biol. Cell.* 41:43–50.

Hiller, G., and K. Weber. 1978. Radioimmunoassay for tubulin: a quantitative comparison of the tubulin content of different established tissue culture cells and tissues. *Cell.* 14:795–804.

Horio, T., and H. Hotani. 1986. Visualization of the dynamic instability of individual microtubules by dark-field microscopy. *Nature (Lond.).* 321:605–607.

Inoué, S., and H. Sato. 1967. Cell motility by labile association of molecules. *J. Gen. Physiol.* 50:259–292.

Keith, C. H., J. R. Feramisco, and M. Shelanski. 1981. Direct visualization of fluorescein-labeled microtubules in vitro and in microinjected fibroblasts. *J. Cell Biol.* 88:234–240.

Kilmartin, J. V., B. Wright, and C. Milstein. 1982. Rat monoclonal antitubulin antibodies derived by using a new nonsecreting rat cell line. *J. Cell Biol.* 93:576–582.

Kristofferson, D., T. Mitchison, and M. Kirschner. 1986. Direct observation of steady-state microtubule dynamics. *J. Cell Biol.* 102:1007–1019.

Kuriyama, R. 1976. *In vitro* polymerization of flagellar and ciliary outer fiber tubulin into microtubules. *J. Biochem. (Tokyo).* 80:153–165.

Laemmli, U. K. 1970. Cleavage of structural proteins during the assembly of the head of bacteriophage T_4. *Nature (Lond.).* 227:680–685.

Lai, E. Y., C. Walsh, D. Wardell, and C. Fulton. 1979. Programmed appearance of translatable flagellar tubulin mRNA during cell differentiation in *Naegleria. Cell.* 17:867–878.

Linck, R. W., and G. L. Langevin. 1981. Reassembly of flagellar B (αβ) tubulin into singlet microtubules: consequences for cytoplasmic microtubule structure and assembly. *J. Cell Biol.* 89:323–337.

Little, M., G. Krämmer, M. Singhofer-Wowra, and R. F. Luduena. 1986. Evolutionary aspects of tubulin structure. *Ann. NY Acad. Sci.* 466:8–12.

Lowry, O. H., N. J. Rosebrough, A. L. Farr, and R. J. Randall. 1951. Protein measurement with the Folin phenol reagent. *J. Biol. Chem.* 193:265–275.

Maekawa, S., and H. Sakai. 1978. Characterization and *in vitro* polymerization of *Tetrahymena* tubulin. *J. Biochem. (Tokyo).* 83:1065–1075.

McKeithan, T. W., and J. L. Rosenbaum. 1981. Multiple forms of tubulin in the cytoskeletal and flagellar microtubules of *Polytomella. J. Cell Biol.* 91:352–360.

Mitchison, T. 1985. Microtubules can incorporate subunits at the kinetochore both in vitro and in vivo. *In* Microtubules and Microtubule Inhibitors. M. De Brabander and J. De Mey, editors. Elsevier Science Publishers B.V., Amsterdam. 111–118.

Mitchison, T., and M. Kirschner. 1984*a*. Microtubule assembly nucleated by isolated centrosomes. *Nature (Lond.).* 312:232–237.

Mitchison, T., and M. Kirschner. 1984*b*. Dynamic instability of microtubules growth. *Nature (Lond.).* 312:237–242.

Mitchison, T. J., and M. W. Kirschner. 1985*a*. Properties of the kinetochore in vitro. I. Microtubule nucleation and tubulin binding. *J. Cell Biol.* 101:755–765.

Mitchison, T. J., and M. W. Kirschner. 1985*b*. Properties of the kinetochore in vitro. II. Microtubule capture and ATP-dependent translocation. *J. Cell Biol.* 101:766–777.

Mitchison, T., L. Evans, E. Schulze, and M. Kirschner. 1986. Sites of microtubule assembly and disassembly in the mitotic spindle. *Cell.* 45:515–527.

Pickett-Heaps, J. D., D. H. Tippit, and K. R. Porter. 1982. Rethinking mitosis. *Cell.* 29:729–744.

Rieder, C. L. 1982. The formation, structure, and composition of the mammalian kinetochore and kinetochore fiber. *Int. Rev. Cytol.* 79:1–58.

Roos, U. P. 1976. Light and electron microscopy of rat kangaroo cells in mitosis. III. Patterns of chromosome behaviour during prometaphase. *Chromosoma (Berl.).* 54:363–385.

Salmon, E. D., R. J. Leslie, W. M. Saxton, M. L. Karow, and J. R. McIntosh. 1984. Spindle microtubule dynamics in sea urchin embryos: analysis using a fluorescein-labeled tubulin and measurements of fluorescence redistribution after laser photobleaching. *J. Cell Biol.* 99:2165–2174.

Sammak, P. J., and G. G. Borisy. 1988. Direct observation of microtubule dynamics in living cells. *Nature (Lond.).* 332:724–726.

Sammak, P. J., G. J. Gorbsky, and G. G. Borisy. 1987. Microtubule dynamics in vivo: a test of mechanisms of turnover. *J. Cell Biol.* 104:395–405.

Saxton, W. M., D. L. Stemple, R. J. Leslie, E. D. Salmon, M. Zavortink, and J. R. McIntosh. 1984. Tubulin dynamics in cultured mammalian cells. *J. Cell Biol.* 99:2175–2186.

Schulze, E., and M. Kirschner. 1986. Microtubule dynamics in interphase cells. *J. Cell Biol.* 102:1020–1031.

Sheir-Neiss, G., R. V. Nardi, M. A. Gealt, and N. R. Morris. 1976. Tubulin-like protein from *Aspergillus nidulans. Biochem. Biophys. Res. Commun.* 69:285–290.

Soltys, B. J., and G. G. Borisy. 1985. Polymerization of tubulin in vivo: direct evidence for assembly onto microtubule ends and from centrosomes. *J. Cell Biol.* 100:1682–1689.

Sonneborn, T. M. 1970. Methods in *Paramecium* research. *Methods Cell Physiol.* 4:241–339.

Sonneborn, T. M. 1974. *Paramecium aurelia. In* Handbook of Genetics. Vol. 2. R. C. King, editor. Plenum Press, New York. 469–594.

Spitzer, J. 1986. Cloning and characterization of an α-tubulin gene in *Paramecium tetraurelia*. Master of Science Thesis. Indiana University, Bloomington, IN. 31–33.

Telzer, B. R., and L. T. Haimo. 1981. Decoration of spindle microtubules with dynein: evidence for uniform polarity. *J. Cell Biol.* 89:373–378.

Towbin, H., T. Staehelin, and J. Gordon. 1979. Electrophoretic transfer of proteins from polyacrylamide gels to nitrocellulose sheets: procedure and some applications. *Proc. Natl. Acad. Sci. USA.* 76:4350–4354.

Wadsworth, P., and E. D. Salmon. 1986. Analysis of the treadmilling model during metaphase of mitosis using fluorescence redistribution after photobleaching. *J. Cell Biol.* 102:1032–1038.

Water, R. D., and L. J. Kleinsmith. 1976. Identification of α and β tubulin in yeast. *Biochem. Biophys. Res. Commun.* 70:704–708.

Weeks, D. P., and P. S. Collis. 1976. Induction of microtubule protein synthesis in *Chlamydomonas reinhardtii* during flagellar regeneration. *Cell.* 9:15–27.

White, J. G., W. B. Amos, and M. Fordham. 1987. An evaluation of confocal versus conventional imaging of biological structures by fluorescence light microscopy. *J. Cell Biol.* 105:41–48.

Witt, P. L., H. Ris, and G. G. Borisy. 1980. Origin of kinetochore microtubules in Chinese hamster ovary cells. *Chromosoma (Berl.).* 81:483–505.